

Kondo physics in carbon nanotubes

Jesper Nygård*, David Henry Cobden†, & Poul Erik Lindelof*

*Ørsted Laboratory, Niels Bohr Institute, Universitetsparken 5, DK-2100 Copenhagen, Denmark

†Department of Physics, University of Warwick, Coventry CV4 7AL, UK

The connection of electrical leads to wire-like molecules is a logical step in the development of molecular electronics, but also allows studies of fundamental physics. For example, metallic carbon nanotubes¹ are quantum wires that have been found to act as one-dimensional quantum dots^{2,3}, Luttinger-liquids^{4,5}, proximity-induced superconductors^{6,7} and ballistic⁸ and diffusive⁹ one-dimensional metals. Here we report that electrically-contacted single-wall nanotubes can serve as powerful probes of Kondo physics, demonstrating the universality of the Kondo effect. Arising in the prototypical case from the interaction between a localized impurity magnetic moment and delocalized electrons in a metallic host, the Kondo effect has been used to explain¹⁰ enhanced low-temperature scattering from magnetic impurities in metals, and also occurs in transport through semiconductor quantum dots¹¹⁻¹⁸. The far higher tunability of dots (in our case, nanotubes) compared with atomic impurities renders new classes of Kondo-like effects^{19,20} accessible. Our nanotube devices differ from previous systems in which Kondo effects have been observed, in that they are one-dimensional quantum dots with three-dimensional metal (gold) reservoirs. This allows us to observe Kondo resonances for very large electron number (N) in the dot, and approaching the unitary limit (where the transmission reaches its maximum possible value). Moreover, we detect a previously unobserved Kondo effect, occurring for even values of N in a magnetic field.

Each of our devices²¹ contains a metallic single-walled nanotube with gold source and drain contacts and a substrate gate contact, as illustrated in Fig. 1a. Several measures are taken to optimize electrical contact between the gold and the nanotubes (see Methods). The resulting two-terminal linear-response conductance G ranges up to more than $3e^2/h$ (resistance 8 k Ω) at room temperature, where h is Planck's constant and e is the electronic charge. We believe this is the highest reported yet for a single-walled tube²². This implies that the transmission probability P of each contact can reach about 0.9 (the maximum theoretical conductance of a metallic tube is¹ $4e^2/h$), demonstrating that nearly ideal contacts are achievable between a normal metal and a molecule. Meanwhile, the variation of P from device to device allows the investigation of different transport regimes.

For $P \ll 1$, as is well established^{2,3}, Coulomb blockade occurs at low temperature T and the device behaves as a one-dimensional (1D) quantum dot²³. The values of the charging energy, U (the average interaction between two electrons), and the average level spacing, ΔE , found for this type of device are as expected for a tube segment of effective length L equal to the contact spacing³. At higher T , the device exhibits a power-law variation of G with T , which can be well explained by Luttinger-liquid behaviour⁴. At the other extreme, for $P \approx 0.9$, we see no Coulomb blockade, and instead the characteristics²¹ resemble those of a diffusive 1D wire even for $T < 1$ K.

It is the intermediate transmission regime which we focus on here. The measurements in Fig. 1 were made on a device having $G \approx 1.6 e^2/h$ (we estimate $P \sim 0.6$) at room temperature. At low T , G undergoes large, reproducible fluctuations as a function of substrate gate voltage V_g (Fig. 1b). Fig. 1c shows the variation with T over a narrower range of V_g . At $T = 780$ mK, the fluctuations are regular and can be identified as Coulomb blockade oscillations. However, unlike normal Coulomb blockade, as T is decreased G decreases in some valleys, marked above with an E, while it increases in other valleys, marked with an O. Fig. 1d shows a greyscale plot of the differential conductance dI/dV vs source-drain bias V and V_g at $T \sim 75$ mK. The enhanced conductance in the O valleys corresponds to the dark (high dI/dV) horizontal features at $V = 0$, such as those labelled X and Y. No such lines are seen in the E valleys, which are instead bounded by roughly hexagonal

bubbles. Although the distinctness of these features varies with V_g , O- and E-type valleys can be seen to alternate for as many as ten consecutive peaks.

These features can be explained by invoking the Kondo effect¹¹⁻¹³. When the number N of electrons on the dot is odd, the total spin S is a half-integer, and second-order processes such as that shown on the left of Fig. 1f can occur. Similar processes, which change the total spin of the dot, add up coherently to form a correlated many-electron state in which electrons in the two leads are strongly coupled, allowing current flow even under blockade conditions if $T < T_K$, the Kondo temperature. When N is even, however, there is no equivalent process, and thus no current, if $S = 0$. This matches the data if in the O valleys N is odd and $S = 1/2$ while in the E valleys N is even and $S = 0$. Further evidence confirming that features X and Y in Fig. 1d are ‘‘Kondo ridges’’ is provided by the logarithmic dependence¹⁶ of G on T in the centers of the ridges, shown in Fig. 1e, and by the splitting of the ridges in a magnetic field (see later).

This new Kondo system differs in several important ways from the two-dimensional (2D) semiconductor dots in which Kondo physics was previously studied.¹⁴⁻¹⁹ First, for semiconductor dots the leads are 2D electron systems, while for tube dots they are normal 3D metal (gold). Second, the excitation spectrum of an interacting 1D dot, which behaves as a Luttinger liquid when Coulomb blockade is overcome⁴, is profoundly different from a 2D dot. Third, since semiconductor dots are electrostatically defined, their geometry and contact transmission probabilities depend on gate voltages. In contrast, for tube dots the contacts cannot be individually tuned, but the fixed geometry means that signs of the Kondo effect can be seen over the entire range of V_g , encompassing hundreds of Coulomb oscillations. Fourth, the effect of a magnetic field is entirely through spin in single-walled nanotube dots, while orbital effects are often dominant in semiconductor dots. Fifth, thanks to this fact combined with the absence of spin-orbit coupling, unlike for a semiconductor dot the spin of a tube dot is well defined and easily measured^{24,25} even for large N . Sixth and last, the conditions^{14,23} on the size L for observing the Kondo effect are weaker in the tube dot. Halfway along a Kondo ridge, $T_K \sim (\Gamma U)^{1/2} \exp[-(\pi/4)U/\Gamma]$, where Γ is the level width. The ratio U/Γ cannot be made smaller than $U/\Delta E$, because $\Gamma < \Delta E$ for any quantum dot. For 2D semiconductor dots, $U/\Delta E \propto L$, so that the maximum possible T_K decreases exponentially with L . This requires them to be made as small as possible, so limiting the electron number N to less than ~ 100 . In contrast, for tube dots, which are 1D, $U/\Delta E \sim 6$ is independent³ of length L , and the maximum T_K decreases only with the prefactor $(\Gamma U)^{1/2}$. This helps to explain how tube dots can show such a strong and clear Kondo effect, even for large N . An order of magnitude estimate of N is the number of π -electrons in the tube, ie, the number of carbon atoms, which is tens of thousands. (Without knowing the exact dot size or band structure a more accurate estimate is not possible.) Nanotube quantum dots therefore allow the first ever observations of the Kondo effect in the limit of very large N .

The width Γ varies from level to level, so we can search for pairs of peaks with particularly large Γ , such as those illustrated in Figs. 2a and 2b. For both these pairs the valley between the peaks is completely gone at base temperature (~ 75 mK). In the Kondo regime, G is expected to saturate at the unitary limit G_0 as $T \rightarrow 0$, and at higher T it should follow a universal scaling form¹⁰ which can be approximated by¹⁵ $G(T) = G_0 / (1 + (2^{1/s} - 1)(T/T_K)^2)^s$, where $s = 0.22$ for spin $1/2$ on the dot. To test this, we fit G vs T in the valley center to this expression using T_K and G_0 as fitting parameters. The results, shown in Fig. 2c, are highly satisfactory. For both peak pairs we find $G_0 > 1.7e^2/h$, which is close to the maximum value of $2e^2/h$ obtained for symmetric coupling to the two contacts (this assumes the double Fermi-point degeneracy¹ is broken). The deduced values of T_K of 1.6 K and 0.9 K are in good agreement with nonlinear measurements, as indicated in the insets above Figs. 2a and 2b. Here, on top of greyscale plots of dI/dV showing the Kondo ridges are superimposed traces of dI/dV vs V midway along each ridge. The Kondo effect is expected to be suppressed¹³ on a bias scale $|V| \sim k_B T_K / e$. Indeed, we see that the width of each peak in dI/dV is roughly $2k_B T_K / e$ (indicated by the vertical white bars). We believe these first measurements on a nanotube dot are closer to the unitary limit than has ever been reported in a semiconductor quantum dot.

In some regions of V_g , such as that shown in Fig. 3, a regular series of faint diamonds can be discerned. This resembles the standard behaviour of a quantum dot for $P \ll 1$, where only first-order tunnelling is significant and Coulomb blockade forces N to be fixed at an integer within the diamonds. However, superimposed on the diamonds are a variety of horizontal features which can be attributed to higher-order tunnelling processes that are strong in this device because P is large. Kondo ridges are seen at $V=0$ in the odd- N diamonds (marked \circ again), which are outlined by white dashed lines. Additional horizontal ridges are seen at $V \neq 0$, such as those labelled \mathbf{P} in the even and \mathbf{Q} in the odd diamonds. Features of type \mathbf{P} truncate every even diamond, resulting in the characteristic alternating bubble-ridge pattern seen also in Fig. 1d. It is natural to associate a horizontal feature at a bias $V = \Delta/e$ with processes generating an excitation of energy Δ in the dot. An example of such a process is cotunneling involving two nondegenerate single-particle states, as sketched on the right of Fig. 3. However, since such inelastic cotunneling normally only produces a step in dI/dV above a threshold, we suggest that these peaks in dI/dV at finite bias offsets are another manifestation of Kondo physics.

Finally, we look at the effect of magnetic field B . Fig. 4a shows the evolution with B of an adjacent bubble (\mathbf{E}) and Kondo ridge (\mathbf{O}). As expected,¹³ the Kondo ridge splits linearly into components at $V = \pm g\mu_B B/e$ (the Zeeman energy), where μ_B is the Bohr magneton and $g = 2.0$ is the electron g -factor^{2,25}. Meanwhile, the edges of the bubble move linearly towards $V = 0$. Fig. 4b shows the dI/dV characteristics in the center of the bubble. At a certain field, $B_c = 1.18$ T, the bubble collapses to a single ridge, corresponding to a peak in dI/dV at $V = 0$. Its T dependence is shown in Fig. 4c. The peak height is logarithmic in T (Fig. 4d), just as for the odd- N Kondo ridge at $B = 0$. A similar ridge is formed in most bubbles at a field dependent on the bubble width at $B = 0$.

Exactly such behaviour has recently been predicted²⁰ for quantum dots when N is even, in the case where the Zeeman energy is sufficiently large. It is assumed that at $B = 0$ the ground state is a singlet ($S = 0$), and the lowest excited state is a triplet ($S = 1$) at a distance Δ_{t-s} above the ground state. In an applied field $B_c = \Delta_{t-s}/g\mu_B$, the $S_z = -1$ member of the triplet becomes degenerate with the singlet (see Fig. 4e). At this point, S alternates between 1 and 0 as electrons cotunnel between the contacts (see Fig. 4f), resulting in a new type of Kondo resonance²⁰ with similar characteristics to the conventional type seen at $B = 0$. This theory is particularly appropriate to single-walled nanotubes, where the effects of B are almost entirely through spin. Applying the model, we deduce for instance that the edges of the \mathbf{E} bubble in Fig. 4a are associated with a singlet-triplet excitation of energy $\Delta_{t-s} = g\mu_B B_c = 137 \mu\text{eV}$.

Note that this new type of Kondo effect is distinct from the one recently discovered in a semiconductor dot¹⁹, which occurs when a singlet is aligned with a *degenerate* triplet by orbital effects in a weak magnetic field. It serves to underline the fact that new physical phenomena can emerge in the study of molecular nanostructures.

Methods

In making devices, the as-grown single-walled nanotube material²⁶ is sonicated in dichloroethane and deposited on the SiO_2 by diluting with isopropyl alcohol before drying. To improve the contacts: the leads are fabricated as soon as possible after tube deposition by low-energy (10 kV) electron-beam lithography; the polymethylmethacrylate resist is over-exposed to avoid residue; the contact metallization is pure gold, evaporated directly on top of the tubes; and each contact covers at least $0.5 \mu\text{m}$ of the tube/bundle. Although we cannot resolve the difference between a single tube and a thin bundle of tubes in the atomic force microscope, we study only devices whose detailed characteristics imply that the conduction is determined by a single metallic nanotube²¹.

References

1. Dekker, C. Carbon Nanotubes as Molecular Quantum Wires. *Physics Today* **52**, 22-28 (1999).

2. Tans, S. *et al.* Individual single-walled carbon nanotubes as quantum wires. *Nature* **386**, 474-477 (1997).
3. Bockrath, M. *et al.* Single-Electron Transport in Ropes of Carbon Nanotubes. *Science* **275**, 1922-1925 (1997).
4. Bockrath, M. *et al.* Luttinger-liquid behaviour in carbon nanotubes. *Nature* **397**, 598-601 (1999).
5. Yao, Z., Postma, H. W. C., Balents, L. & Dekker, C. Carbon nanotube intramolecular junctions. *Nature* **402**, 273-276 (1999).
6. Kasumov, A. Y. *et al.* Supercurrents Through Single-Walled Carbon Nanotubes. *Science* **284**, 1508-1511 (1999).
7. Morpurgo, A. F., Kong, J., Marcus, C. & Dai, H. Gate-Controlled Superconducting Proximity Effect in Carbon Nanotubes. *Science* **286**, 263-265 (1999).
8. Frank, S., Poncharal, S. P., Wang, Z. L. & de Heer, W. A. Carbon Nanotube Quantum Resistors. *Science* **280**, 1744-1746 (1998).
9. Bachtold, A. *et al.* Aharonov-Bohm oscillations in carbon nanotubes. *Nature* **397**, 673-675 (1999).
10. Hewson, A. C. *The Kondo Problem to Heavy Fermions* (Cambridge University Press, Cambridge, 1993).
11. Glazman, L. I. & Raikh, M. E. Resonant Kondo transparency of a barrier with quasilocal impurity states. *JETP Lett.* **47**, 452-455 (1988).
12. Ng, T. K. & Lee, P. A. On-site Coulomb repulsion and resonant tunneling. *Phys. Rev. Lett.* **61**, 1768-1771 (1988).
13. Meir, Y., Wingreen, N. S. & Lee, P. A. Low-Temperature Transport Through a Quantum Dot: The Anderson Model Out of Equilibrium. *Phys. Rev. Lett.* **70**, 2601-2604 (1993).
14. Goldhaber-Gordon, D., Shtrikman, H., Mahalu, D., Abusch-Magder, D., Meirav, U. & Kastner, M. A. Kondo effect in a single-electron transistor. *Nature* **391**, 156-159 (1998).
15. Goldhaber-Gordon, D. *et al.* From the Kondo Regime to the Mixed-Valence Regime in a Single-Electron Transistor. *Phys. Rev. Lett.* **81**, 5225-5228 (1998).
16. Cronenwett, S. M., Oosterkamp, T. H. & Kouwenhoven, L. P. A Tuneable Kondo Effect in Quantum Dots. *Science* **281**, 540-544 (1998).
17. Schmid, J., Weis, J., Eberl, K. & v. Klitzing, K. A quantum dot in the limit of strong coupling to reservoirs. *Physica B* **256-258**, 182-185 (1998).
18. Simmel, F., Blick, R. H., Kotthaus, J. P., Wegscheider, W. & Bichler, M. Anomalous Kondo Effect in a Quantum Dot at Nonzero Bias. *Phys. Rev. Lett.* **83**, 804-807 (1999).
19. Sasaki, S. *et al.* A novel Kondo effect in an integer-spin quantum dot. *Nature* **405**, 764-767 (2000).
20. Pustilnik, M., Avishai, Y. & Kikoin, K. Quantum Dots with Even Number of Electrons: Kondo Effect in a Finite Magnetic Field. *Phys. Rev. Lett.* **84**, 1756-1759 (2000).
21. Nygård, J., Cobden, D. H., Bockrath, M., McEuen, P. L. & Lindelof, P. E. Electrical transport measurements on single-walled carbon nanotubes. *Appl. Phys. A* **69**, 297-304 (1999).
22. Soh, H. T. *et al.* Integrated nanotube circuits: Controlled growth and ohmic contacting of single-walled carbon nanotubes. *Appl. Phys. Lett.* **75**, 627-629 (1999).
23. Glazman, L. I. Single Electron Tunneling. *J. Low Temp. Phys.* **118**, 247-269 (2000).
24. Tans, S., Devoret, M. H., Groeneveld, R. J. A. & Dekker, C. Electron-electron correlations in carbon nanotubes. *Nature* **394**, 761-764 (1998).
25. Cobden, D. H., Bockrath, M., McEuen, P. L., Rinzler, A. G. & Smalley, R. E. Spin Splitting and Even-Odd Effects in Carbon Nanotubes. *Phys. Rev. Lett.* **81**, 681-684 (1998).
26. Thess, A. *et al.* Crystalline Ropes of Metallic Carbon Nanotubes. *Science* **273**, 483-487 (1996).

Acknowledgements. We thank A. Rinzler and R. Smalley for supplying the nanotubes, K. G. Rasmussen, M. M. Andreassen, A. E. Hansen and A. Kristensen for experimental assistance, and M. Pustilnik, N. Wingreen, L. P. Kouwenhoven, N. d'Ambrumenil, P. R. Poulsen and P. L. McEuen for helpful discussions.

Correspondence should be addressed to D.H.C. (email: d.h.cobden@warwick.ac.uk).

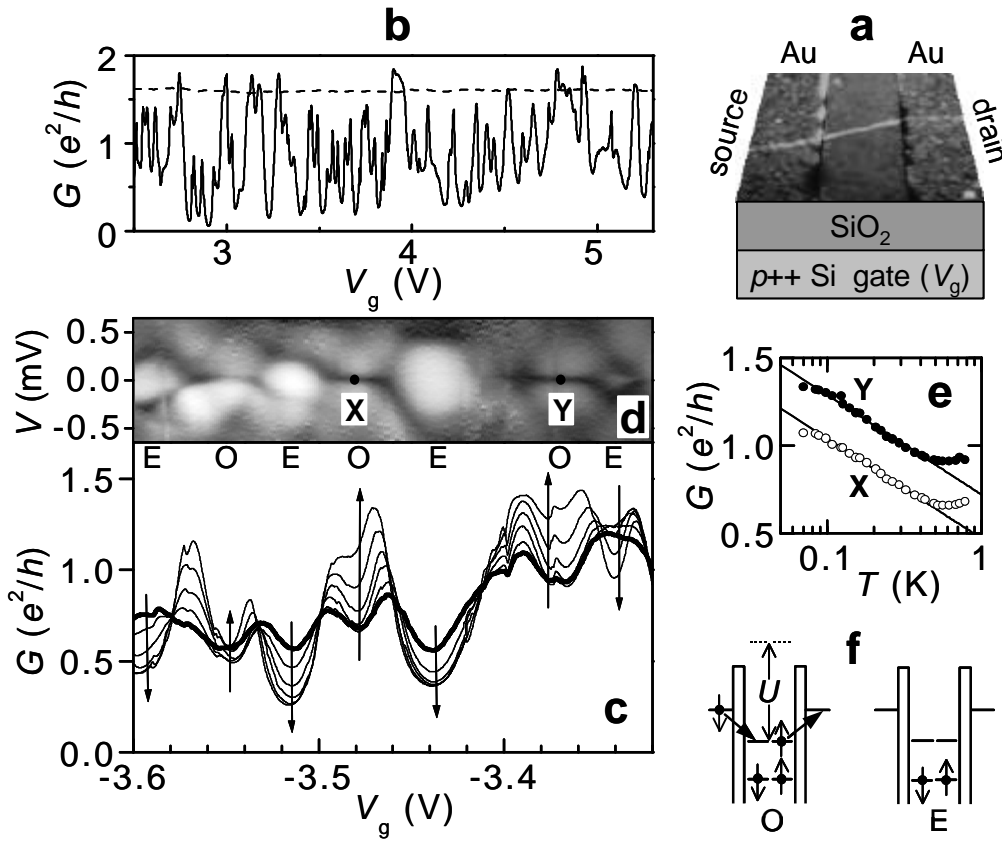


Figure 1. Characteristics of a nanotube device with intermediate contact transmission probabilities. **a** Device consisting of a 2 nm-thick nanotube bundle with 30 nm-thick gold contacts separated by 300 nm. Sketched beneath the tapping-mode atomic force microscope (AFM) image are the 300-nm thick SiO_2 layer and the highly p -doped Si substrate used as the gate electrode. **b** At room temperature (dashed line) the linear-response conductance G is about $1.6 e^2/h$, almost independent of gate voltage V_g . At $T \approx 75$ mK, the base electron temperature on our dilution refrigerator, reproducible fluctuations are seen in G vs V_g . (The source-drain bias V used was $7 \mu\text{V}$ dc). **c** Temperature dependence of a narrower region of V_g . $T = 75, 125, 180, 245, 320, 490, 560$, and (thicker line) 780 mK. Vertical arrows indicate the direction of change with decreasing T , which is opposite in the regions labelled E and O. **d** Greyscale plot of dI/dV against V and V_g , over the same region of V_g (darker = more positive). **e** Conductance vs temperature at points X and Y in panel (d). The straight lines indicate $\log(T)$ behaviour. **f** Interpretation of the situation in the O and E regions. In O regions the number of electrons N on the dot is odd, and higher-order spin-flipping processes can occur, leading to a Kondo resonance. In the E regions N is even and no such processes exist.

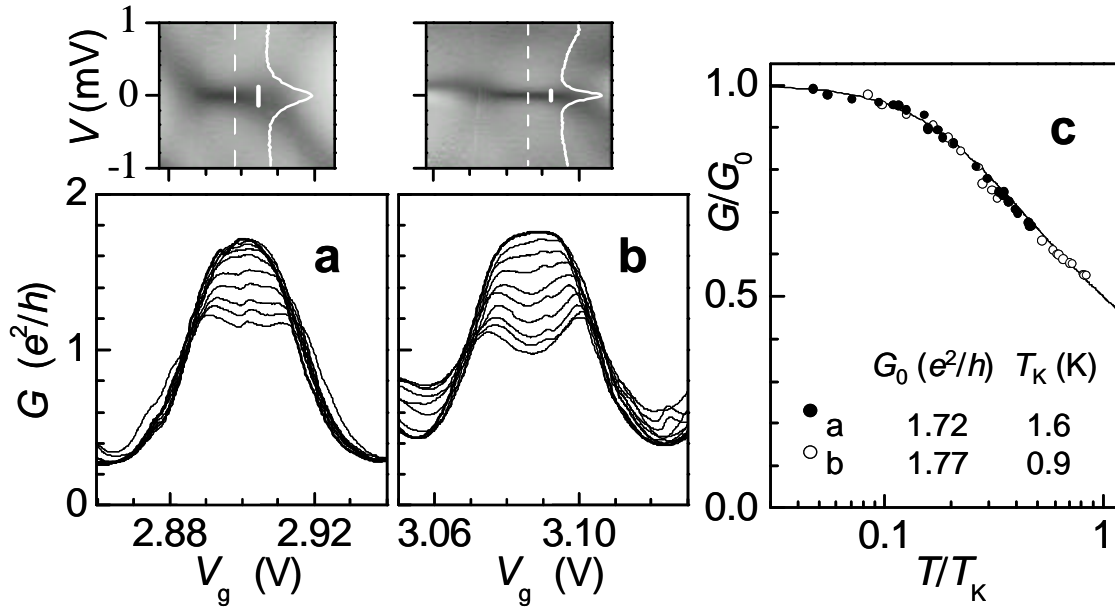


Figure 2. Analysis of two high-conductance peak pairs. **a** and **b** Temperature dependence of G vs V_g . $T = 75$ (thick line), 87, 150, 200, 250, 330, 420, 530, 630 and 740 mK. Above are dI/dV greyscales at 75 mK in the same regions of V_g , showing broad Kondo ridges. Superimposed on each is the dI/dV vs V trace along the dashed line, which also serves to denote $dI/dV = 0$. The vertical white bars are of length $2k_B T_K/e$, where T_K is obtained in each case from the data in panel (c). **c** G vs T data in the valley centers for the peak pairs in panels (a) and (b), scaled in each case to match the theoretical scaling function given in the text (solid line). The deduced values of G_0 and T_K are given.

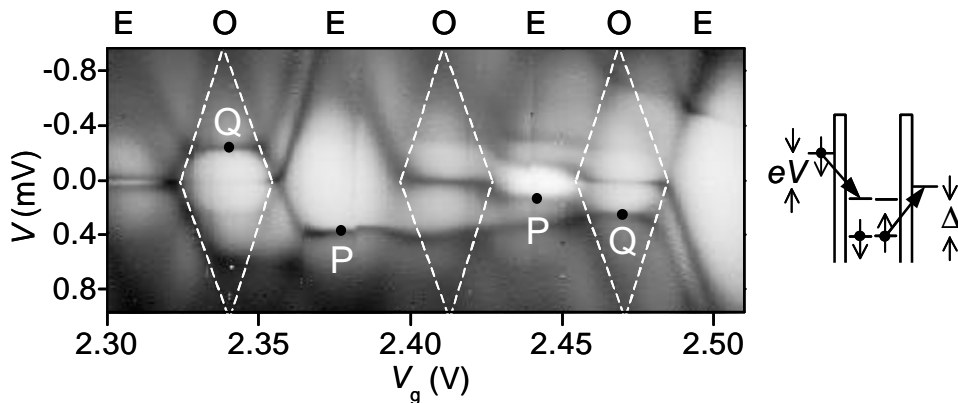


Figure 3. dI/dV greyscale plot in a different V_g region at $T = 75$ mK. Dashed lines outline the odd Coulomb diamonds. Horizontal features such as those labelled P and Q suggest higher-order processes like the second-order one sketched on the right, where tunneling involves two levels separated by an energy Δ and occurs only for bias $V \geq \Delta/e$.

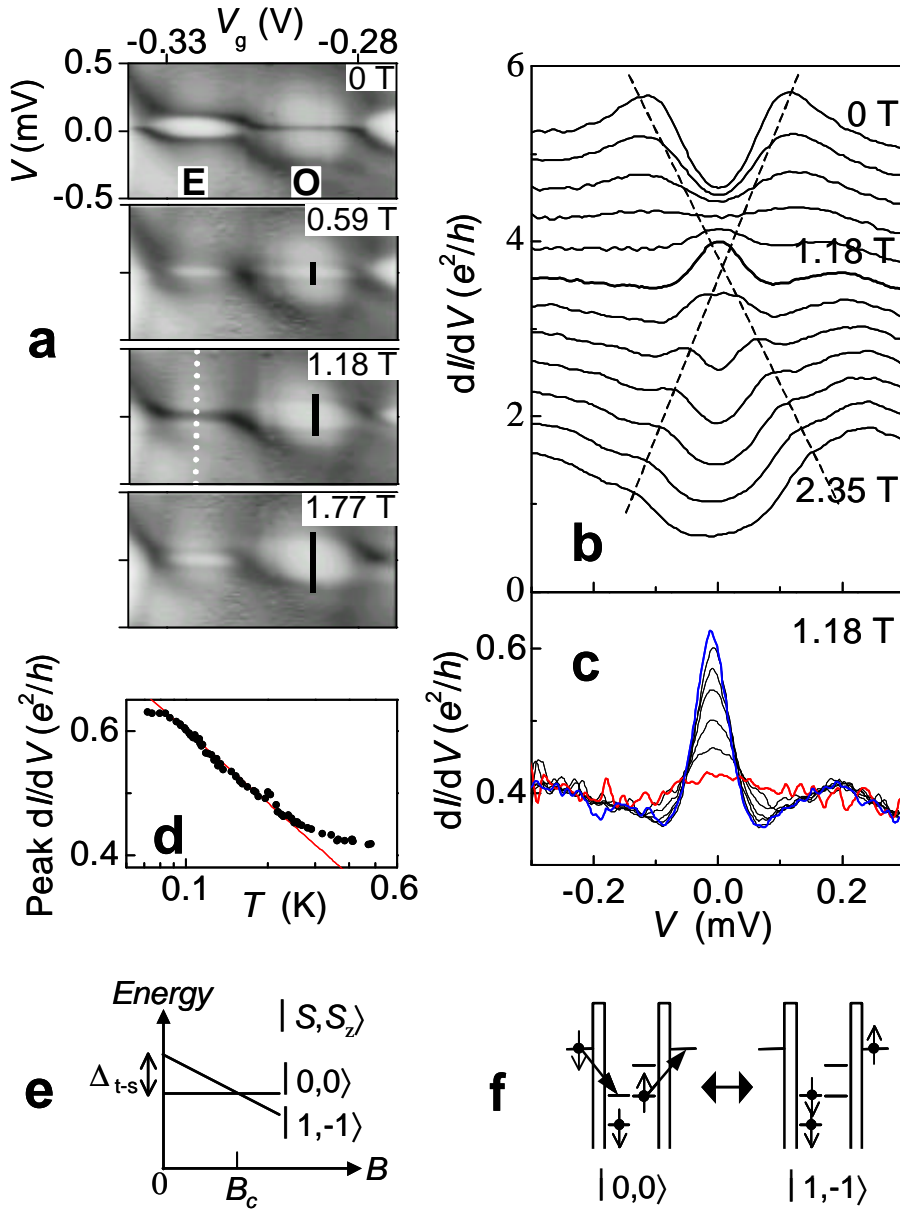


Figure 4. Effect of perpendicular magnetic field B . **a** dI/dV greyscale plot at $T = 75$ mK showing adjacent odd- N (O) and even- N (E) regions at a series of fields. The vertical bars have length $2g_{\mu_B}B/e$. As B increases the O ridge splits while the E bubble shrinks to a single ridge at 1.18 T before reappearing at higher B . **b** Evolution of dI/dV characteristics at $V_g = -0.322$ V (indicated by the white dotted line in (a)) at $T = 75$ mK. The traces are offset from each other by $0.4 e^2/h$ for clarity. The dashed lines, which indicate the motion of the peaks, are sloped according to $g_{\mu_B}B/e$. **c** Temperature dependence of the peak in dI/dV at $B = 1.18$ T. $T = 75$ (blue), 100, 115, 130, 180, 230, and 350 mK (red). **d** Peak value of dI/dV (at $V = 0$) plotted against $\log(T)$. **e** A singlet $|S, S_z\rangle = |0, 0\rangle$ ground state becomes degenerate with a triplet $|1, -1\rangle$ excited state at $B =$

$B_c = \Delta_{t-s}/g\mu_B$. At this point, spin-flipping higher order transitions, as sketched in **f**, become possible, leading to a new type of Kondo resonance.